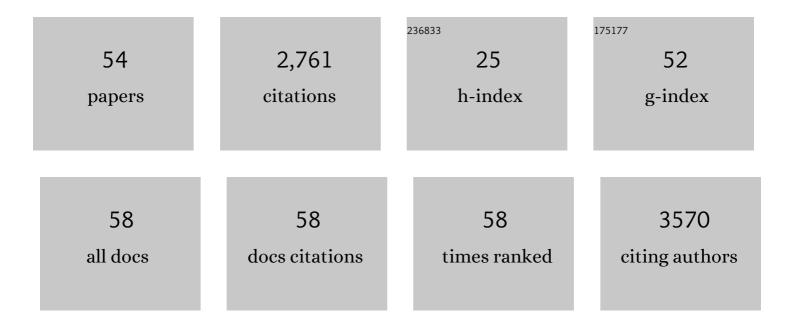
Jing Zhang

List of Publications by Year in descending order

Source: https://exaly.com/author-pdf/1580627/publications.pdf Version: 2024-02-01



ΙΝΟ ΖΗΛΝΟ

#	Article	IF	CITATIONS
1	Progress of nanocrystalline growth kinetics based on oriented attachment. Nanoscale, 2010, 2, 18-34.	2.8	486
2	Removal of Antibiotic Florfenicol by Sulfide-Modified Nanoscale Zero-Valent Iron. Environmental Science & Technology, 2017, 51, 11269-11277.	4.6	251
3	A Multistep Oriented Attachment Kinetics:Â Coarsening of ZnS Nanoparticle in Concentrated NaOH. Journal of the American Chemical Society, 2006, 128, 12981-12987.	6.6	194
4	Treatment of Cr ^{VI} ontaining Mg(OH) ₂ Nanowaste. Angewandte Chemie - International Edition, 2008, 47, 5619-5622.	7.2	175
5	Adsorption and coadsorption mechanisms of Cr(VI) and organic contaminants on H3PO4 treated biochar. Chemosphere, 2017, 186, 422-429.	4.2	133
6	Environmentally persistent free radicals mediated removal of Cr(VI) from highly saline water by corn straw biochars. Bioresource Technology, 2018, 260, 294-301.	4.8	131
7	Redox Reactions between Mn(II) and Hexagonal Birnessite Change Its Layer Symmetry. Environmental Science & Technology, 2016, 50, 1750-1758.	4.6	102
8	Heavy metal chemical extraction from industrial and municipal mixed sludge by ultrasound-assisted citric acid. Journal of Industrial and Engineering Chemistry, 2015, 27, 368-372.	2.9	87
9	Rapid removal of organic pollutants by activation sulfite with ferrate. Chemosphere, 2017, 186, 576-579.	4.2	74
10	Oriented Attachment Kinetics for Ligand Capped Nanocrystals:Â Coarsening of Thiol-PbS Nanoparticles. Journal of Physical Chemistry B, 2007, 111, 1449-1454.	1.2	68
11	Microscopic mechanism about the selective adsorption of Cr(VI) from salt solution on O-rich and N-rich biochars. Journal of Hazardous Materials, 2021, 404, 124162.	6.5	63
12	Pure multistep oriented attachment growth kinetics of surfactant-free SnO2 nanocrystals. Physical Chemistry Chemical Physics, 2009, 11, 8516.	1.3	53
13	Simultaneous redox conversion and sequestration of chromate(VI) and arsenite(III) by iron(III)-alginate based photocatalysis. Applied Catalysis B: Environmental, 2019, 259, 118046.	10.8	46
14	Simultaneous photocatalytic redox removal of chromium(<scp>vi</scp>) and arsenic(<scp>iii</scp>) by hydrothermal carbon-sphere@nano-Fe ₃ O ₄ . Environmental Science: Nano, 2019, 6, 937-947.	2.2	44
15	Visible-light photocatalysis accelerates As(III) release and oxidation from arsenic-containing sludge. Applied Catalysis B: Environmental, 2019, 250, 1-9.	10.8	43
16	Hierarchical Core–Shell Co ₂ N/CoP Embedded in N, Pâ€doped Carbon Nanotubes as Efficient Oxygen Reduction Reaction Catalysts for Znâ€air Batteries. Small, 2022, 18, e2108094.	5.2	39
17	Smectic phase in suspensions of gapped DNA duplexes. Nature Communications, 2016, 7, 13358.	5.8	38
18	Growth and Phase-Transformation Mechanisms of Nanocrystalline CdS in Na ₂ S Solution. Journal of Physical Chemistry C, 2008, 112, 9229-9233.	1.5	37

Jing Zhang

#	Article	IF	CITATIONS
19	Evolution of ZnS Nanostructure Morphology under Interfacial Free-Energy Control. Chemistry of Materials, 2008, 20, 2438-2443.	3.2	34
20	NaOH Concentration Effect on the Oriented Attachment Growth Kinetics of ZnS. Journal of Physical Chemistry B, 2007, 111, 5290-5294.	1.2	32
21	Enhanced removal of antimony by acid birnessite with doped iron ions: Companied by the structural transformation. Chemosphere, 2019, 226, 834-840.	4.2	32
22	Structure and dynamics of water in nonionic reverse micelles: A combined time-resolved infrared and small angle x-ray scattering study. Journal of Chemical Physics, 2012, 137, 044503.	1.2	31
23	Emerging investigator series: treatment and recycling of heavy metals from nanosludge. Environmental Science: Nano, 2019, 6, 1657-1673.	2.2	31
24	The Effects of Particle Concentration and Surface Charge on the Oriented Attachment Growth Kinetics of CdTe Nanocrystals in H ₂ O. Journal of Physical Chemistry C, 2011, 115, 10357-10364.	1.5	27
25	Adsorption Mechanisms of Dodecylbenzene Sulfonic Acid by Corn Straw and Poplar Leaf Biochars. Materials, 2017, 10, 1119.	1.3	27
26	Electrocatalytic reduction of Cr(VI) over heterophase MoS2 film electrode. Chemical Engineering Journal, 2021, 404, 126556.	6.6	25
27	Modified Local Soil (MLS) Technology for Harmful Algal Bloom Control, Sediment Remediation, and Ecological Restoration. Water (Switzerland), 2019, 11, 1123.	1.2	24
28	Removal of organic dye by biomass-based iron carbide composite with an improved stability and efficiency. Journal of Hazardous Materials, 2019, 369, 621-631.	6.5	23
29	Direct Visualization of Conformation and Dense Packing of DNA-Based Soft Colloids. Physical Review Letters, 2014, 113, 268303.	2.9	22
30	Enhanced degradation performance of p-chlorophenol in photo-Fenton reaction activated by nano-FeO encapsulated in hydrothermal carbon: Improved Fe(III)/Fe(II) cycle. Colloids and Surfaces A: Physicochemical and Engineering Aspects, 2020, 594, 124650.	2.3	21
31	Simultaneous oxidation of Cr(III) and extraction of Cr(VI) from chromite ore processing residue by silicate-assisted hydrothermal treatment. Chemical Engineering Journal, 2019, 371, 565-574.	6.6	20
32	Experimental determination of resolution function parameters from small-angle neutron scattering data of a colloidal SiO ₂ dispersion. Journal of Applied Crystallography, 2010, 43, 686-692.	1.9	19
33	Hydrothermal treatment of arsenic sulfide slag to immobilize arsenic into scorodite and recycle sulfur. Journal of Hazardous Materials, 2021, 406, 124735.	6.5	19
34	Synthesis and Self-Assembly of Squarelike PbCrO ₄ Nanoplatelets via Micelle-Mediated Depletion Attraction. Langmuir, 2013, 29, 4679-4687.	1.6	18
35	Electrocatalytical oxidation of arsenite by reduced graphene oxide via in-situ electrocatalytic generation of H2O2. Environmental Pollution, 2019, 254, 112958.	3.7	18
36	Relationship between the coprecipitation mechanism, doping structure and physical properties of Zn1â^'xCoxS nanocrystallites. Nanotechnology, 2007, 18, 035705.	1.3	16

Jing Zhang

#	Article	lF	CITATIONS
37	Formation and Self-Assembly of Cadmium Hydroxide Nanoplates in Molten Composite-Hydroxide Solution. Crystal Growth and Design, 2010, 10, 4285-4291.	1.4	16
38	Optimization and calculation of the LaBr3–MBr (M=Na, K, Rb, Cs) phase diagrams. Calphad: Computer Coupling of Phase Diagrams and Thermochemistry, 2004, 28, 147-151.	0.7	15
39	Synthesis of Bi ₂ WO ₆ /Na-bentonite composites for photocatalytic oxidation of arsenic(<scp>iii</scp>) under simulated sunlight. RSC Advances, 2019, 9, 29689-29698.	1.7	13
40	Thermodynamic optimization of the CeCl3–AECl2 (AE=Mg,Ca,Sr,Ba) phase diagrams. Calphad: Computer Coupling of Phase Diagrams and Thermochemistry, 2003, 27, 305-308.	0.7	12
41	The Mass Production of ZnS Nanoarchitecture via Thermodynamic Design. Crystal Growth and Design, 2008, 8, 2324-2328.	1.4	12
42	Cellulose Mediated Reduction and Immobilization of Cr(VI) in Chromite Ore Processing Residue. Journal of Hazardous Materials, 2020, 394, 122538.	6.5	12
43	Effective photocatalytic removal of As(III) by ZnFe2O4/Ag/AgCl coupled peroxymonosulfate: Z-Scheme charge transfer and dual active sites. Applied Surface Science, 2021, 567, 150860.	3.1	11
44	A novel layer-layer crossed structure of bentonite/g-C3N4 for enhanced photocatalytic oxidation of arsenic(III) in a wide pH range. Surfaces and Interfaces, 2021, 26, 101365.	1.5	9
45	Visible-light activation of sulfite by ZnFe2O4@PANI photocatalyst for As(III) removal: The role of radicals and Fe(IV). Applied Surface Science, 2022, 578, 151940.	3.1	9
46	Chemical and spectroscopic characteristics of humic acid from a clay loam soil in Ontario after 52 years of consistent fertilization and crop rotation. Pedosphere, 2021, 31, 204-213.	2.1	7
47	DNA Self-Assembly Mediated by Programmable Soft-Patchy Interactions. ACS Nano, 2020, 14, 13524-13535.	7.3	6
48	Enrichment of sulfur-oxidizing bacteria using S-doped NiFe2O4 nanosheets as the anode in microbial fuel cell enhances power production and sulfur recovery. Science of the Total Environment, 2022, 844, 156973.	3.9	6
49	Self-assembly of biaxial discorectangular lead carbonate nanosheets into stacked ribbons studied by SAXS and HAADF-STEM tomographic tilt series. Soft Matter, 2014, 10, 9511-9522.	1.2	5
50	PH-dependent photochemical transformation of arsenic sulfide sludge catalyzed by Fe ions under visible light irradiation. Applied Catalysis B: Environmental, 2021, 293, 120186.	10.8	5
51	Thermodynamic optimization of DyCl3-NaCl system. Journal of Shanghai University, 2005, 9, 279-282.	0.1	3
52	Controllable synthesis and self-assembly of PbCO3 nanorods in shape-dependent nonionic w/o microemulsions. Soft Matter, 2013, 9, 7576.	1.2	3
53	Sorption behavior of dodecylbenzene sulfonic acid on humic acids from Mollisol and Alluvial soils. Environmental Earth Sciences, 2016, 75, 1.	1.3	3
54	Formation of amorphous PbCrO ₄ nanoparticles depending on the quantitative control of interfacial water. Molecular Systems Design and Engineering, 2021, 6, 918-924.	1.7	0